NASA TECHNICAL NOTE

NASA TN D-3639

NASA TN D-3639

EXPERIMENTAL AND THEORETICAL RESULTS FOR BUCKLING OF ECCENTRICALLY STIFFENED CYLINDERS

by Michael F. Card and Robert M. Jones

Langley Research Center
Langley Station, Hampton, Va.

NATIONAL AERONAUTICS AND SPACE ADMINISTRATION • WASHINGTON, D. C. • OCTOBER 1966

EXPERIMENTAL AND THEORETICAL RESULTS FOR BUCKLING OF ECCENTRICALLY STIFFENED CYLINDERS

By Michael F. Card and Robert M. Jones

Langley Research Center
Langley Station, Hampton, Va.

NATIONAL AERONAUTICS AND SPACE ADMINISTRATION

For sale by the Clearinghouse for Federal Scientific and Technical Information
Springfield, Virginia 22151 – Price $1.00

EXPERIMENTAL AND THEORETICAL RESULTS FOR BUCKLING OF ECCENTRICALLY STIFFENED CYLINDERS[1]

By Michael F. Card and Robert M. Jones
Langley Research Center

SUMMARY

Results from an experimental and theoretical study of the effect of stiffener eccentricity (one-sidedness) on buckling are reported. In the experimental investigation, axial-compression tests were conducted on twelve longitudinally stiffened cylinders which represent six configurations with internal or external, integral or Z-stiffeners. For certain configurations externally stiffened cylinders were found to carry over twice the load sustained by their internally stiffened counterparts. A solution was obtained by a Galerkin procedure for buckling of clamped, eccentrically stiffened, orthotropic cylinders under axial compression, lateral pressure, or hydrostatic pressure. The experimental results for axially loaded cylinders range from 70 to 95 percent of the corresponding theoretical predictions. However, it is concluded from the comparison that a membrane prebuckled shape is sufficient for assessment of eccentricity effects. Furthermore, comparison of solutions for clamped and simply supported cylinders with the test data and with previous theoretical results reveals that edge clamping has a significant effect.

INTRODUCTION

The influence of eccentricity or one-sidedness of stiffeners on the buckling strength of stiffened cylindrical shells has been demonstrated in several studies (refs. 1 to 6). Buckling predictions derived from these studies indicate that the magnitude of the eccentricity effects can be very substantial for certain configurations. Unfortunately, few experiments have been devised to verify the trends of those theories. A need consequently exists for buckling test data on eccentrically stiffened cylinders. Furthermore, correlation of test data with available theory is limited because the theoretical boundary conditions usually considered are simple support whereas the test cylinders may have nearly clamped edges.

---

[1]A part of the material presented herein is contained in the proceedings of AIAA/ASME Seventh Structures and Materials Conference (Cocoa Beach, Florida), April 18-20, 1966, pp. 23-34, under the title "Buckling of Axially Compressed Cylinders With Eccentric Longitudinal Stiffeners," by Michael F. Card and Robert M. Jones.

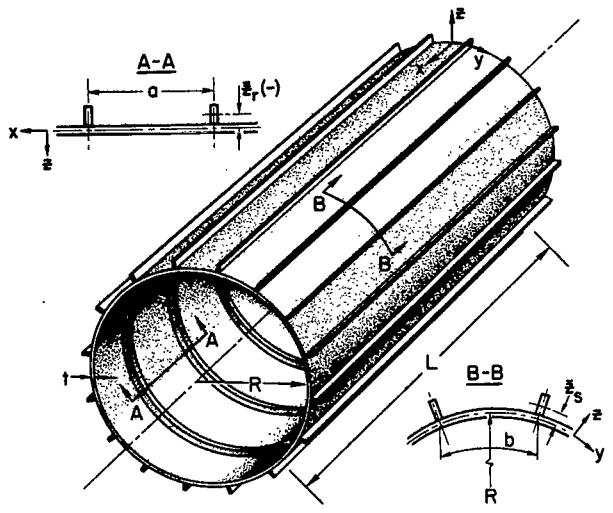

Figure 1.- Stiffened-cylinder configuration.

The purpose of the present paper is to report the results of an experimental and theoretical study of the effects of stiffener eccentricity on the buckling strength of stiffened cylinders. (See fig. 1 for configuration.) In the experimental investigation, axial-compression tests were conducted on twelve longitudinally stiffened cylinders which represent six configurations with internal or external integral or Z-stiffeners. Preliminary results of the experimental investigation are reported in reference 7.

In the present paper, the test results are compared with theoretical predictions for simply supported and clamped cylinders in order to assess the effect of boundary conditions on the buckling load. The theoretical predictions are based on the buckling theory given in reference 6. The theory presented therein is a generalization of that given in reference 2. The solution for simply supported edges is reported in reference 6 and the solution for clamped edges obtained by use of a Galerkin procedure is reported in appendix A of this paper. The solution in appendix A is valid for clamped, eccentrically stiffened, orthotropic cylinders under axial compression, lateral pressure, or hydrostatic pressure. Some additional results on the influence of boundary conditions are presented in appendix B.

SYMBOLS

The units for the physical quantities defined in this paper are given both in U.S. Customary Units and in the International System of Units (SI) (ref. 8). Factors relating these two systems are presented in appendix C.

a ring spacing (see fig. 1)

A cross-sectional area of stiffener

A_t total cross-sectional area of stiffeners and cylinder

b stringer spacing (see fig. 1)

D bending stiffness of isotropic plate, $\frac{Et^3}{12(1 - \mu^2)}$

D_x, D_y bending stiffnesses of orthotropic cylinder in longitudinal and circumferential directions, respectively

D_{xy} twisting stiffness of orthotropic cylinder

E Young's modulus

E_x, E_y extensional stiffnesses of orthotropic cylinder in longitudinal and circumferential directions, respectively

G shear modulus, $\frac{E}{2(1 + \mu)}$

G_{xy} in-plane shear stiffness of orthotropic cylinder

h height of stiffener element

I moment of inertia about centroid of stiffener

J torsional constant for stiffener, $\sum t_{se}^3 h\left(\frac{1}{3} - \frac{64}{\pi^5}\frac{t_{se}}{h}\tanh\frac{\pi h}{2t_{se}}\right)$ (see ref. 9)

k_x axial-compression stress coefficient, $\frac{\sigma t L^2}{D\pi^2}$

L cylinder length

m number of longitudinal buckle half-waves

M_x additional moment per unit length during buckling

n number of circumferential buckle waves

n_e experimental value of n

N_x additional axial force per unit length of circumference during buckling

$\bar{N}_x, \bar{N}_y$ applied axial and circumferential forces per unit length, respectively

$\bar{N}_e$ experimental value of $\bar{N}_x$

$\bar{N}_c$ theoretical value of $\bar{N}_x$ for clamped edges

$\bar{N}_s$	theoretical value of $\bar{N}_x$ for simply supported edges
p_c	corrugation width (see fig. 2)
$\bar{P}_e$	experimental value of axial buckling force
R	radius of cylinder middle surface
t	cylinder thickness
$\bar{t}$	effective thickness of stiffened isotropic cylinder, $\frac{A_r}{a} + t$ or $\frac{A_s}{b} + t$
t_c	corrugation thickness (see fig. 2)
t_{se}	thickness of stiffener element
u,v,w	displacements from membrane prebuckled shape in longitudinal, circumferential, and radial directions, respectively
x,y,z	longitudinal, circumferential, and radial coordinates, respectively
Z	curvature parameter, $\frac{L^2}{Rt}\sqrt{1 - \mu^2}$
$\bar{z}$	distance from stiffener centroid to cylinder middle surface (see fig. 1), positive when stiffener on outside
ϵ	axial strain
σ	axial stress
$\bar{\sigma}_e$	experimental average axial buckling stress
θ_c	corrugation angle (see fig. 2)
μ	Poisson's ratio
μ_x, μ_y	Poisson's ratios for bending of orthotropic cylinder in longitudinal and circumferential directions, respectively

μ'_x, μ'_y Poisson's ratios for extension of orthotropic cylinder in longitudinal and circumferential directions, respectively

Subscripts:

r,s denote properties of rings (circumferential stiffening) and stringers (longitudinal stiffening), respectively

When the subscripts x and y follow a comma, they indicate partial differentiation of the principal symbol with respect to x and y.

EXPERIMENTAL INVESTIGATION OF LONGITUDINALLY STIFFENED CYLINDERS

Specimens

Buckling data and stress-strain curves were obtained for twelve longitudinally stiffened cylinders. Four specimens of about 9.55-inch (24.26-cm) radius and about 0.0279-inch (0.0709-cm) thickness employed integral rectangular stiffeners; eight specimens of about 15.92-inch (40.44-cm) radius and about 0.0399-inch (0.1013-cm) thickness employed Z-stiffeners which were riveted to the cylinder. For each configuration, two identical cylinders were constructed, one with external stiffening and the other with internal stiffening. All specimens were designed with closely spaced stiffeners to preclude local buckling of the cylinder. Construction details are given in figure 2 and table I.

The cylinders with integral rectangular stiffeners were machined from 3/8-inch (0.95-cm) aluminum plates. The dimensions given in table I were obtained by careful measurement. The cylinder thickness t is the average of a large number of micrometer measurements. The scatter in individual thicknesses was ±8 percent of the tabulated value and is attributed to difficulties in measurement on the specimen surface. Note in table I, however, that the average-thickness values are fairly uniform. There were two butt joints per cylinder, each with two doubler plates 0.70 inch (1.78 cm) wide and 0.020 inch (0.064 cm) thick fastened to the cylinder with a single row of 3/32-inch (0.24-cm) rivets spaced at 5/16 inch (0.79 cm) on each side of the joint.

The Z-stiffened cylinders were nominally identical to certain test specimens discussed in reference 10 except that the Z-stiffeners were located on the external surface of the present specimens, whereas in reference 10 the Z-stiffeners were located on the internal surface. Four externally stiffened cylinders were tested to complement the results of the four comparable internally stiffened cylinders reported in reference 10. All dimensions are nominal except the area of the stiffened cylinder cross section A_t,

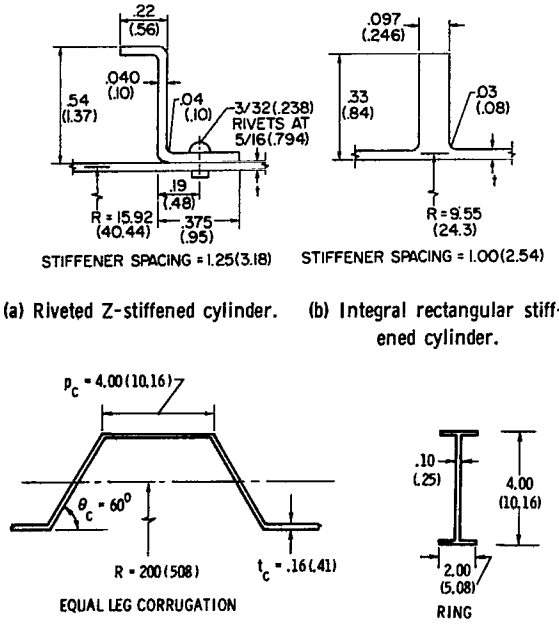

(a) Riveted Z-stiffened cylinder. (b) Integral rectangular stiffened cylinder.

(c) Ring-stiffened, corrugated cylinder.

Figure 2.- Dimensions of stiffened cylinder cross sections. All dimensions are in inches (centimeters).

which was determined by weighing and the cylinder thickness t, which was obtained by micrometer measurements. Individual cylinder thicknesses were within the usual tolerances specified for rolled sheet. There were three lap joints 3/4 inch (1.91 cm) wide, each with a double row of 3/32-inch (0.24-cm) rivets spaced at 5/16-inch (0.79-cm) intervals. The rivet spacing for the stringers was also 5/16 inch (0.79 cm).

Procedure

The cylinders were loaded in axial compression in the 1,200-kip-capacity (5.3-MN) universal static testing machine at the Langley Research Center. The ends of the cylinders were ground flat and parallel after being potted in a soft, low-temperature alloy for ease in machining. The cylinders were carefully alined in the testing machine to insure uniform bearing between the ends of the cylinders and the platens of the testing machine. Circularity of the cylinders was maintained during the tests by the use of 1/4-inch-thick (0.64-cm) aluminum bulkheads which were held in place by the potting material at each end of the cylinder.

Twelve resistance-wire strain gages with a 6-inch (15-cm) gage length were mounted in back-to-back pairs on the cylinder and on the stringers to determine stress distribution and to detect buckling. The overall shortening of the distance between the testing machine platens was measured with the use of strain gages mounted on a small cantilever beam, the fixed end of which was fastened to the lower platen. A long rod connected the beam to the upper platen shown in figure 3(a) so that the shortening of the cylinder was equal to the deflection of the cantilever. The strain and shortening measurements were recorded during the test at a virtually continuous rate on the Langley central digital data recording system.

Stress Distribution

Stress-strain curves derived from the strain-gage data for each of the test cylinders are presented for stresses below the buckling stress in figure 4. The strain plotted is that measured at the location which experienced the maximum strain during the test. The value of the strain corresponds to the average of data from a pair of back-to-back

TABLE I.- DIMENSIONS AND RESULTS

(a) U.S. Customary Units

Cylinder	Aluminum alloy	Type of stiffener	Stiffener location	t, in.	L, in.	R, in.	A_t, in^2	$\overline{P}_e$, kips	$\bar{\sigma}_e$, ksi	n_e	$\overline{N}_e$, kips/in.	$\overline{N}_c$, kips/in.	$\overline{N}_s$, kips/in.
1	2024-T351*	Integral	External	0.0283	38.00	9.55	3.69	112.6	30.5	6	1877	2036	1145
2	2024-T351*	Integral	Internal	.0277	38.00	9.55	3.72	48.0	12.9	6	800	997	687
3	2024-T351*	Integral	External	.0275	23.75	9.55	3.70	127.2	34.4	7	2120	2595	1326
4	2024-T351*	Integral	Internal	.0280	23.75	9.55	3.63	58.0	16.0	6	965	1226	722
5	7075-T6*	Z	External	.0410	59.00	15.92	7.15	169.6	23.7	5	1696	2289	1193
6**	7075-T6*	Z	Internal	.0401	59.00	15.92	7.25	99.5	13.7	6	995	1174	766
7	7075-T6*	Z	External	.0391	41.83	15.92	7.02	186.3	26.6	7	1863	2617	1283
8**	7075-T6*	Z	Internal	.0401	41.83	15.92	7.31	126.0	17.2	6	1260	1383	773
9	7075-T6*	Z	External	.0392	29.68	15.92	7.06	273.0	38.7	7	2730	3426	1574
10**	7075-T6*	Z	Internal	.0403	29.68	15.92	7.21	171.0	23.7	7	1710	1813	838
11	7075-T6*	Z	External	.0395	20.77	15.92	7.18	378.0	52.6	8	3780	4947	2068
12**	7075-T6*	Z	Internal	.0401	20.77	15.92	7.18	273.0	38.1	8	2730	2845	1027

*$E = 10.5 \times 10^3$ ksi; $\mu = 0.32$.

**Data are taken from reference 10.

(b) International System of Units

Cylinder	Aluminum alloy	Type of stiffener	Stiffener location	t, cm	L, cm	R, cm	A_t, cm^2	$\overline{P}_e$, kN	$\bar{\sigma}_e$, MN/m^2	n_e	$\overline{N}_e$, MN/m	$\overline{N}_c$, MN/m	$\overline{N}_s$, MN/m
1	2024-T351*	Integral	External	0.0719	96.5	24.26	23.8	500	210	6	329	357	200
2	2024-T351*	Integral	Internal	.0704	96.5	24.26	24.0	214	89	6	140	175	120
3	2024-T351*	Integral	External	.0699	60.3	24.26	23.9	566	237	7	371	454	232
4	2024-T351*	Integral	Internal	.0711	60.3	24.26	23.4	258	110	6	169	215	127
5	7075-T6*	Z	External	.1041	149.9	40.44	46.1	754	163	5	297	401	209
6**	7075-T6*	Z	Internal	.1019	149.9	40.44	46.8	443	94	6	174	206	134
7	7075-T6*	Z	External	.0993	106.2	40.44	45.3	829	183	7	326	458	225
8**	7075-T6*	Z	Internal	.1019	106.2	40.44	47.2	560	119	6	221	242	135
9	7075-T6*	Z	External	.0996	75.4	40.44	45.5	1214	267	7	478	600	276
10**	7075-T6*	Z	Internal	.1024	75.4	40.44	46.5	761	163	7	299	317	147
11	7075-T6*	Z	External	.1003	52.8	40.44	46.3	1681	363	8	662	866	362
12**	7075-T6*	Z	Internal	.1019	52.8	40.44	46.3	1214	263	8	478	498	180

*$E = 72\ 400\ MN/m^2$; $\mu = 0.32$.

**Data are taken from reference 10.

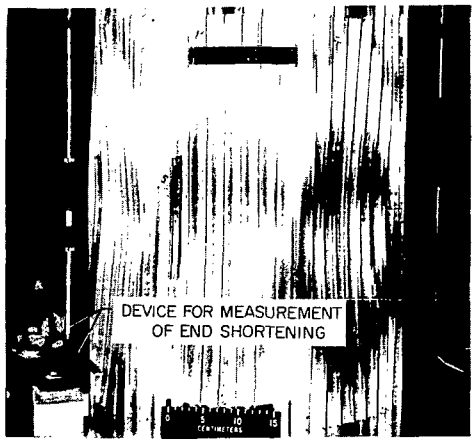

(a) Integrally stiffened cylinder no. 3.

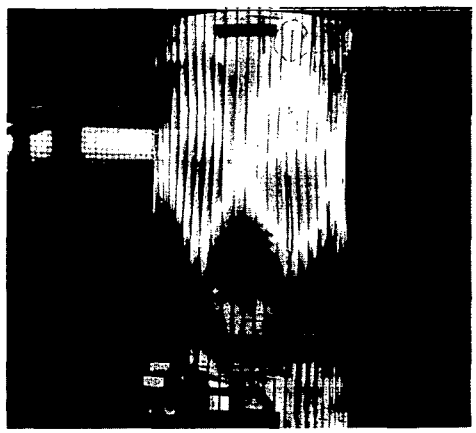

(b) Integrally stiffened cylinder no. 1.

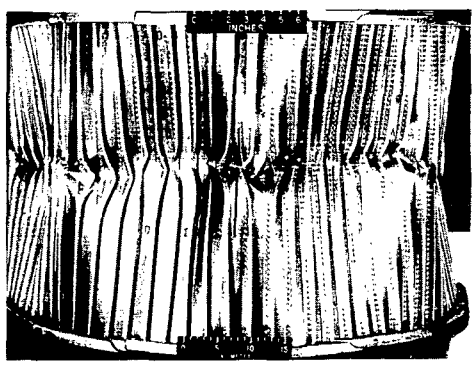

(c) Z-stiffened cylinder no. 11.

Figure 3.- Buckled cylinders. L-66-4432

gages mounted on the stiffeners or cylinder. The strain distribution was nearly uniform for all tests. Individual strain-gage readings at loads near buckling differed at most by 10 percent of the plotted values. Strains measured in back-to-back gages prior to buckling differed by about $1\frac{1}{2}$ percent of their average value.

All the stress-strain curves of figure 4 are linear up to at least 85 percent of the maximum stress carried by the cylinder. The slopes of the linear portion of the curves are in reasonable agreement with conventional values of Young's modulus. Slopes of the load-shortening curves derived from the average of the cantilever measurements were also in agreement with accepted modulus values. The strain data indicate no local buckling of the cylinders prior to general buckling. The data also indicate that, for all cylinders except cylinder 4, the buckling load and maximum load could be considered identical. For cylinder 4, strain reversal occurred at 94 percent of the maximum load and was considered to determine the buckling load.

Buckling

For the externally stiffened cylinders, buckling was accompanied by a loud report and the appearance of several diamond-shaped buckles of large amplitude. In contrast, for the internally stiffened cylinders, buckling was a milder phenomenon with similar buckles of smaller amplitude. Photographs of buckled cylinders are shown in figure 3. The diamond-shaped buckles occurred in only one tier in all cases except cylinder 1 for which two tiers developed. (Compare figs. 3(a) and 3(b).) The number of circumferential waves n_e into which the cylinders buckled experimentally is shown in table I.

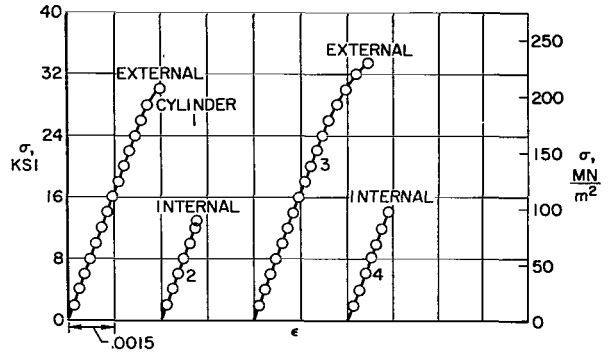

(a) Integrally stiffened cylinders.

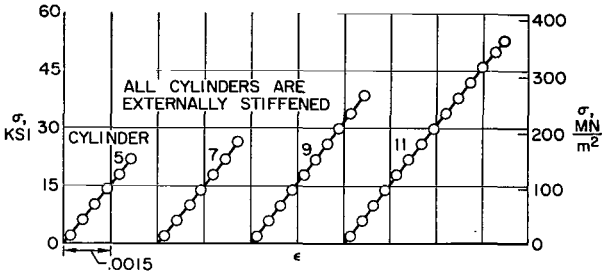

(b) Z-stiffened cylinders.

Figure 4.- Stress-strain curves.

The buckling loads together with the corresponding average axial compressive stresses carried by the cylinder at buckling are given in table I. Data for cylinders 6, 8, 10, and 12 from reference 10 are included for comparative purposes. Examination of the buckling loads reveals that, for the test boundary conditions, locating the longitudinal stiffening on the external surface of the cylinder can produce a significant increase (to over twice as much) in axial load-carrying ability over that of the comparable internally stiffened cylinder.

THEORETICAL RESULTS AND COMPARISON OF THEORY AND EXPERIMENT FOR LONGITUDINALLY STIFFENED CYLINDERS

The influence of the boundary conditions of the present longitudinally stiffened cylinders must be considered because the cylinders are effectively short as will be seen subsequently herein. For this reason, the experimental results are compared with buckling predictions from solutions for cylinders which have, in one case, simply supported edges and, in the other, clamped edges. The calculations for simply supported cylinders were obtained by employing equation (15) of reference 6, the boundary conditions of which can be identified as $N_x = v = w = M_x = 0$. The calculations for clamped

cylinders ($u = v = w = w_{,x} = 0$) were obtained from the solution in appendix A. Note especially the difference in axial constraint between the two sets of boundary conditions.

The solution for clamped cylinders presented in appendix A is based on the stability differential equations of reference 6 wherein a membrane prebuckled state was utilized. The buckling displacements, u, v, and w, were expanded in trigonometric series, each term of which satisfies the clamped-edge boundary conditions. A generalized Galerkin procedure was applied to obtain a set of algebraic equations which only admit solutions for certain values (eigenvalues) of the load parameter. Buckling loads and mode shapes correspond to the lowest eigenvalue and its eigenvector, respectively.

Theoretical and experimental results for integrally stiffened and Z-stiffened cylinders are shown in figures 5 and 6, respectively, and in table I. The theoretical results in figures 5 and 6 are based on the average of the stiffened-cylinder dimensions given in table I. In figures 5 and 6, substantial boundary-condition effects are evident. Note that the percentage difference between the solutions for simply supported and clamped edges is greater for externally stiffened cylinders than for their internally stiffened counterparts. Thus, boundary conditions are more significant for externally than for internally stiffened cylinders of the configurations considered. This result should not be interpreted too generally because the opposite effect is shown in appendix B for certain ring-stiffened corrugated cylinders.

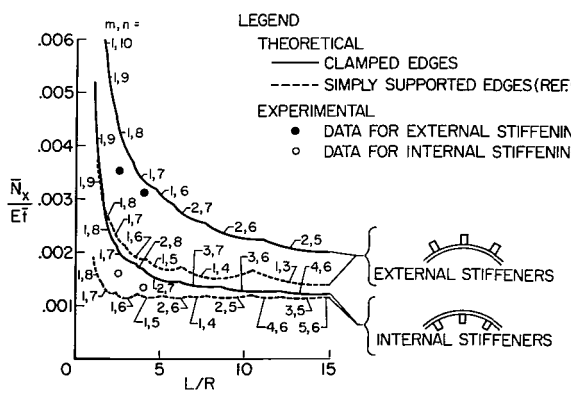

Figure 5.- Buckling of axially compressed integrally stiffened cylinders (as described in table I and fig. 2).

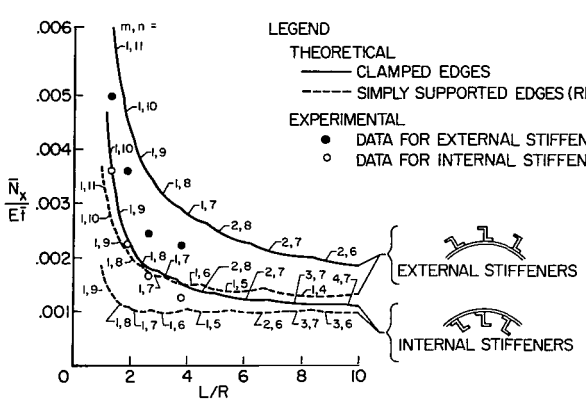

Figure 6.- Buckling of axially compressed Z-stiffened cylinders (as described in table I and fig. 2).

The theoretical buckling results shown in figures 5 and 6 have been extended to large values of the length-radius ratio L/R to investigate the convergence of the solution for clamped edges to the solution for simply supported edges. Note from the figures that even for L/R = 10 substantial boundary-condition effects are present for externally stiffened cylinders. Although it is expected

that boundary conditions have an influence in stiffened cylinders, the actual magnitude of the effects at such large values of L/R is somewhat unexpected. In particular, boundary-condition effects are present in longitudinally stiffened cylinders at values of L/R for which the boundary conditions of unstiffened cylinders have usually been regarded as immaterial. Appendix B shows that the presence of these effects is due in part to the additional axial constraint implied by the present clamped boundary conditions. However, appendix B also indicates that other stiffened configurations have large boundary-condition effects at relatively large values of L/R.

In the course of the theoretical investigation, it was observed that the torsional stiffness G_sJ_s had a much larger influence on the buckling load for integrally stiffened cylinders than for Z-stiffened cylinders. This situation is explained by noting that the integrally stiffened cylinders have a relatively shallow stiffener so that the ratio of twisting to bending stiffness G_sJ_s/E_sI_s is much larger than for the Z-stiffened cylinders. To assess the magnitude of this effect, calculations were made in which G_sJ_s was set equal to zero. Whereas the resulting buckling loads for Z-stiffened cylinders were only 1 percent lower than the loads shown in figure 6, the corresponding values for integrally stiffened cylinders were 10 to 20 percent lower than those shown in figure 5. Thus, for some types of stiffening, it is possible to arrive at erroneous conclusions regarding the behavior of stiffened shells if torsional stiffness is neglected.

In general, the qualitative trends of the theory are verified by the experimental results. Evidently, the test cylinders were more nearly clamped than simply supported. Quantitatively, the experimental data vary from 70 to 95 percent of the theoretical predictions for clamped cylinders. Better agreement occurs for internally than for externally Z-stiffened cylinders and for externally than for internally integrally stiffened cylinders. In addition to boundary conditions, contributions to the difference between theory and experiment can result from neglect of initial imperfections and from the absence of an accurate prebuckling solution in the theory. However, comparison of theoretical and experimental results suggests that use of a membrane prebuckling shape is sufficient for assessment of eccentricity effects.

CONCLUDING REMARKS

The results of an experimental and theoretical study of the effects of stiffener eccentricity on the buckling strength of stiffened cylinders have been discussed. The buckling experiments were conducted on 12 axially compressed, longitudinally stiffened cylinders in order to study the relative effect of locating stiffeners on the internal or external surface of the cylinder. Externally stiffened cylinders were found to carry axial loads up to twice those sustained by their internally stiffened counterparts, a fact which has previously been predicted on theoretical grounds.

The experimental buckling data for axial compression of longitudinally stiffened cylinders have been compared with an existing theoretical solution for simply supported cylinders and with a solution described in an appendix for clamped stiffened cylinders. Quantitatively, the experimental data vary from 70 to 95 percent of the theoretical predictions for clamped cylinders. The comparison indicates that use of a membrane prebuckled shape is sufficient for assessment of eccentricity effects in longitudinally stiffened cylinders. It was also found that for some configurations, the torsional stiffness of stiffeners can have a substantial effect on the buckling load. In addition, large effects of edge clamping and axial constraint were found for stiffened cylinders with length-radius ratios for which unstiffened cylinders are generally considered to be insensitive to boundary conditions.

Langley Research Center,
National Aeronautics and Space Administration,
Langley Station, Hampton, Va., June 7, 1966,
124-11-06-04-23.

APPENDIX A

BUCKLING OF CLAMPED ECCENTRICALLY STIFFENED ORTHOTROPIC CYLINDERS UNDER AXIAL COMPRESSION, LATERAL PRESSURE, OR HYDROSTATIC PRESSURE

The following stability equations for eccentrically stiffened orthotropic cylinders which have the configuration shown in figure 1 are presented in reference 6. The equations are expressed in terms of displacements u, v, and w from a membrane prebuckled shape which has externally applied force resultants $\overline{N}_x$ and $\overline{N}_y$:

$$\left(\frac{E_x}{1 - \mu_x'\mu_y'} + \frac{E_sA_s}{b}\right)u,_{xx} + G_{xy}u,_{yy} + \left(G_{xy} + \frac{\mu_y'E_x}{1 - \mu_x'\mu_y'}\right)v,_{xy} + \frac{\mu_y'E_x}{R\left(1 - \mu_x'\mu_y'\right)}w,_x$$

$$- \bar{z}_s\frac{E_sA_s}{b}w,_{xxx} = 0 \tag{A1}$$

$$\left(\frac{E_y}{1 - \mu_x'\mu_y'} + \frac{E_rA_r}{a}\right)v,_{yy} + G_{xy}v,_{xx} + \left(G_{xy} + \frac{\mu_x'E_y}{1 - \mu_x'\mu_y'}\right)u,_{xy}$$

$$+ \frac{1}{R}\left(\frac{E_y}{1 - \mu_x'\mu_y'} + \frac{E_rA_r}{a}\right)w,_y - \bar{z}_r\frac{E_rA_r}{a}w,_{yyy} = 0 \tag{A2}$$

$$\left(\frac{D_x}{1 - \mu_x\mu_y} + \frac{E_sI_s}{b} + \frac{E_sA_s}{b}\bar{z}_s^2\right)w,_{xxxx} + \left(\frac{\mu_yD_x}{1 - \mu_x\mu_y} + 2D_{xy} + \frac{\mu_xD_y}{1 - \mu_x\mu_y} + \frac{G_sJ_s}{b} + \frac{G_rJ_r}{a}\right)w,_{xxyy}$$

$$+ \left(\frac{D_y}{1 - \mu_x\mu_y} + \frac{E_rI_r}{a} + \frac{E_rA_r}{a}\bar{z}_r^2\right)w,_{yyyy} + \frac{\mu_x'E_y}{R\left(1 - \mu_x'\mu_y'\right)}u,_x - \bar{z}_s\frac{E_sA_s}{b}u,_{xxx}$$

$$+ \frac{1}{R}\left(\frac{E_y}{1 - \mu_x'\mu_y'} + \frac{E_rA_r}{a}\right)v,_y - \bar{z}_r\frac{E_rA_r}{a}v,_{yyy} + \frac{1}{R^2}\left(\frac{E_y}{1 - \mu_x'\mu_y'} + \frac{E_rA_r}{a}\right)w$$

$$+ \left(\overline{N}_y - \frac{2}{R}\bar{z}_r\frac{E_rA_r}{a}\right)w,_{yy} + \overline{N}_xw,_{xx} = 0 \tag{A3}$$

The clamped-edge boundary conditions at $x = 0$ and L chosen for the present investigation are

$$u = v = w = w,_x = 0 \tag{A4}$$

APPENDIX A

A solution which is apparently equivalent to solution of equations (A1) to (A3) with boundary conditions expressed by equation (A4) is obtained by an indirect method in reference 3. For the sake of clarity and completeness, a straightforward solution is obtained here by a generalized Galerkin procedure. (See ref. 11.) The displacements are expanded in a series of functions which satisfy the boundary conditions, equation (A4):

$$\left.\begin{aligned} u &= \sum_i a_i u_i^* = \cos\frac{ny}{R}\sum_{i=1}^{\infty} a_i \sin\frac{i\pi x}{L} \\ v &= \sum_i b_i v_i^* = \sin\frac{ny}{R}\sum_{i=1}^{\infty} b_i \sin\frac{i\pi x}{L} \\ w &= \sum_i c_i w_i^* = \cos\frac{ny}{R}\sum_{i=1}^{\infty} c_i\left[\cos(i-1)\frac{\pi x}{L} - \cos(i+1)\frac{\pi x}{L}\right] \end{aligned}\right\} \tag{A5}$$

The Galerkin procedure requires that the following equations be satisfied:

$$\left.\begin{aligned} \int_0^{2\pi R}\int_0^{L} u_i^* Q_x(u,v,w)\,dx\,dy &= 0 \\ \int_0^{2\pi R}\int_0^{L} v_i^* Q_y(u,v,w)\,dx\,dy &= 0 \\ \int_0^{2\pi R}\int_0^{L} w_i^* Q_z(u,v,w)\,dx\,dy &= 0 \end{aligned}\right\} \tag{A6}$$

where Q_x, Q_y, and Q_z are the left-hand sides of equations (A1), (A2), and (A3) with the series, equations (A5), substituted for u, v, and w, respectively. If I terms are taken in each of the series in equations (A5), then equations (A6) represent a set of 3I linear, homogeneous, algebraic equations in 3I unknowns. The set is symmetric if the reciprocal relations

$$\mu_x' E_y = \mu_y' E_x$$

$$\mu_x D_y = \mu_y D_x$$

are employed. Examination of the resulting equations reveals that the equations with a_i (i odd), b_i (i even), and c_i (i even) are not coupled with those which involve a_i (i even), b_i (i odd), and c_i (i odd). Thus, there are two independent sets of simultaneous equations, one of which represents a symmetric w-deformation (i odd in c_i) and the other an antisymmetric w-deformation (i even in c_i). Both sets can be written as

$$\tilde{A}X = \tilde{B}X \tag{A7}$$

where

$$\tilde{A} = \left[\begin{array}{ccc|ccc|ccc} A_{11} & & & B_{11} & B_{12} & B_{13} \cdots & C_{11} & C_{12} & \\ & A_{22} & & B_{21} & B_{22} & B_{23} \cdots & C_{21} & C_{22} & C_{23} \\ & & A_{33} & B_{31} & B_{32} & B_{33} \cdots & & C_{32} & C_{33} \; C_{34} \\ & & \ddots & \vdots & \vdots & \vdots & & \vdots & \vdots \\ \hline & & & D_{11} & & & E_{11} & E_{12} & E_{13} \cdots \\ & & & & D_{22} & & E_{21} & E_{22} & E_{23} \cdots \\ & & & & & D_{33} & E_{31} & E_{32} & E_{33} \cdots \\ & & & & & \ddots & \vdots & \vdots & \vdots \\ \hline & & & & & & F_{11} & F_{12} & \\ & & & & & & F_{21} & F_{22} & F_{23} \\ & & & & & & & F_{32} & F_{33} \; F_{34} \\ & & & & & & & \vdots & \vdots \end{array}\right] \quad \text{(A8)}$$

(symmetric about main diagonal)

$$\tilde{B} = \left[\begin{array}{ccc|ccc|ccc} & & & & & & & & \\ & \text{(zero)} & & & \text{(zero)} & & & \text{(zero)} & \\ & & & & & & & & \\ \hline & & & & & & & & \\ & & & & \text{(zero)} & & & \text{(zero)} & \\ & & & & & & & & \\ \hline & & & & & & P_{11} & P_{12} & \\ & & & & & & & P_{22} & P_{23} \\ & & & & & & & & P_{33} \; P_{34} \\ & & & & & & & & \ddots \end{array}\right] \quad \text{(A9)}$$

(symmetric about main diagonal)

and

$$X_{\text{symmetric}} = \begin{bmatrix} a_2 \\ a_4 \\ a_6 \\ \vdots \\ \hline b_1 \\ b_3 \\ b_5 \\ \vdots \\ \hline c_1 \\ c_3 \\ c_5 \\ \vdots \end{bmatrix} \qquad X_{\text{antisymmetric}} = \begin{bmatrix} a_1 \\ a_3 \\ a_5 \\ \vdots \\ \hline b_2 \\ b_4 \\ b_6 \\ \vdots \\ \hline c_2 \\ c_4 \\ c_6 \\ \vdots \end{bmatrix} \tag{A10}$$

For the symmetric case, the elements of the submatrices in equations (A8) and (A9) are

$$\left.\begin{aligned}
A_{ij} &= \left(\frac{E_x}{1 - \mu_x'\mu_y'} + \frac{E_S A_S}{b}\right)(2j)^2\left(\frac{\pi}{L}\right)^2 + G_{xy}\left(\frac{n}{R}\right)^2 && (i = j) \\
B_{ij} &= -\frac{8}{L}\frac{n}{R}\frac{i(2j - 1)}{(2i)^2 - (2j - 1)^2}\left(\frac{\mu_x' E_y}{1 - \mu_x'\mu_y'} + G_{xy}\right) && \\
C_{ij} &= -\bar{z}_S\frac{E_S A_S}{b}(2j)^3\left(\frac{\pi}{L}\right)^3 - \frac{\mu_y' E_x}{R\left(1 - \mu_x'\mu_y'\right)}(2j)\frac{\pi}{L} && (i = j) \\
C_{ij} &= \bar{z}_S\frac{E_S A_S}{b}(2j - 2)^3\left(\frac{\pi}{L}\right)^3 + \frac{\mu_y' E_x}{R\left(1 - \mu_x'\mu_y'\right)}(2j - 2)\frac{\pi}{L} && (i = j - 1) \\
C_{ij} &= 0 && (i = j + 1)
\end{aligned}\right\} \tag{A11}$$

(Equations continued on next page)

APPENDIX A

$$D_{ij} = \left(\frac{E_y}{1 - \mu_x'\mu_y} + \frac{E_r A_r}{a}\right)\left(\frac{n}{R}\right)^2 + G_{xy}(2j - 1)^2\left(\frac{\pi}{L}\right)^2 \qquad (i = j)$$

$$E_{ij} = \frac{4}{\pi}(2i - 1)\left[\frac{1}{(2i - 1)^2 - (2j - 2)^2} - \frac{1}{(2i - 1)^2 - (2j)^2}\right]\left[\left(\frac{E_y}{1 - \mu_x'\mu_y'} + \frac{E_r A_r}{a}\right)\frac{n}{R^2} + \bar{z}_r \frac{E_r A_r}{a}\left(\frac{n}{R}\right)^3\right]$$

$$F_{11} = 16\Lambda_1 + 4\Lambda_2 + 3\Lambda_3$$

$$F_{ij} = \left[(2j - 2)^4 + (2j)^4\right]\Lambda_1 + \left[(2j - 2)^2 + (2j)^2\right]\Lambda_2 + 2\Lambda_3 \qquad (i = j \neq 1)$$

$$F_{ij} = -\left[(2j - 2)^4\Lambda_1 + (2j - 2)^2\Lambda_2 + \Lambda_3\right] \qquad (i = j - 1)$$

$$P_{11} = 4\left(\frac{\pi}{L}\right)^2\bar{N}_x + 3\left(\frac{n}{R}\right)^2\bar{N}_y$$

$$P_{ij} = \left[(2j - 2)^2 + (2j)^2\right]\left(\frac{\pi}{L}\right)^2\bar{N}_x + 2\left(\frac{n}{R}\right)^2\bar{N}_y \qquad (i = j \neq 1)$$

$$P_{ij} = -\left[(2j - 2)^2\left(\frac{\pi}{L}\right)^2\bar{N}_x + \left(\frac{n}{R}\right)^2\bar{N}_y\right] \qquad (i = j - 1)$$

(A11) Conc.

where

$$\Lambda_1 = \left(\frac{\pi}{L}\right)^4\left(\frac{D_x}{1 - \mu_x\mu_y} + \frac{E_S I_S}{b} + \frac{E_S A_S}{b}\bar{z}_S^2\right)$$

$$\Lambda_2 = \left(\frac{\pi}{L}\right)^2\left(\frac{n}{R}\right)^2\left(\frac{\mu_y D_x}{1 - \mu_x\mu_y} + 2D_{xy} + \frac{\mu_x D_y}{1 - \mu_x\mu_y} + \frac{G_S J_S}{b} + \frac{G_r J_r}{a}\right)$$

$$\Lambda_3 = \left(\frac{n}{R}\right)^4\left(\frac{D_y}{1 - \mu_x\mu_y} + \frac{E_r I_r}{a} + \frac{E_r A_r}{a}\bar{z}_r^2\right) + \frac{1}{R^2}\left(\frac{E_y}{1 - \mu_x'\mu_y'} + \frac{E_r A_r}{a}\right) + \frac{2\bar{z}_r}{R}\frac{E_r A_r}{a}\left(\frac{n}{R}\right)^2$$

APPENDIX A

For the antisymmetric case, the elements of the submatrices in equations (A8) and (A9) are

$$
\left.
\begin{aligned}
A_{ij} &= \left(\frac{E_x}{1 - \mu_x'\mu_y'} + \frac{E_s A_s}{b}\right)(2j - 1)^2\left(\frac{\pi}{L}\right)^2 + G_{xy}\left(\frac{n}{R}\right)^2 && (i = j)\\
B_{ij} &= -\frac{8}{L}\frac{n}{R}\frac{(2i - 1)j}{(2i - 1)^2 - (2j)^2}\left(\frac{\mu_y' E_x}{1 - \mu_x'\mu_y'} + G_{xy}\right)\\
C_{ij} &= \bar{z}_s \frac{E_s A_s}{b}(2j - 1)^3\left(\frac{\pi}{L}\right)^3 + \frac{\mu_y' E_x}{R\left(1 - \mu_x'\mu_y'\right)}(2j - 1)\frac{\pi}{L} && (i = j)\\
C_{ij} &= 0 && (i = j - 1)\\
C_{ij} &= -\bar{z}_s \frac{E_s A_s}{b}(2j + 1)^3\left(\frac{\pi}{L}\right)^3 - \frac{\mu_y' E_x}{R\left(1 - \mu_x'\mu_y'\right)}(2j + 1)\frac{\pi}{L} && (i = j + 1)\\
D_{ij} &= \left(\frac{E_y}{1 - \mu_x'\mu_y'} + \frac{E_r A_r}{a}\right)\left(\frac{n}{R}\right)^2 + G_{xy}(2j)^2\left(\frac{\pi}{L}\right)^2 && (i = j)\\
E_{ij} &= \frac{8i}{\pi}\left[\frac{1}{(2i)^2 - (2j - 1)^2} - \frac{1}{(2i)^2 - (2j + 1)^2}\right]\left[\left(\frac{E_y}{1 - \mu_x'\mu_y'} + \frac{E_r A_r}{a}\right)\frac{n}{R^2}\right.\\
&\quad \left. + \bar{z}_r \frac{E_r A_r}{a}\left(\frac{n}{R}\right)^3\right]\\
F_{ij} &= \left[(2j - 1)^4 + (2j + 1)^4\right]\Lambda_1 + \left[(2j - 1)^2 + (2j + 1)^2\right]\Lambda_2 + 2\Lambda_3 && (i = j)\\
F_{ij} &= -\left[(2j - 1)^4\Lambda_1 + (2j - 1)^2\Lambda_2 + \Lambda_3\right] && (i = j - 1)\\
P_{ij} &= \left[(2j - 1)^2 + (2j + 1)^2\right]\left(\frac{\pi}{L}\right)^2\bar{N}_x + 2\left(\frac{n}{R}\right)^2\bar{N}_y && (i = j)\\
P_{ij} &= -\left[(2j - 1)^2\left(\frac{\pi}{L}\right)^2\bar{N}_x + \left(\frac{n}{R}\right)^2\bar{N}_y\right] && (i = j - 1)
\end{aligned}
\right\} \quad \text{(A12)}
$$

where Λ_1, Λ_2, and Λ_3 are the same as defined in equations (A11).

APPENDIX A

It is convenient for what follows to further abbreviate equation (A7) as

$$\left[\begin{array}{c|c|c} A & B & C \\ \hline B^T & D & E \\ \hline C^T & E^T & F \end{array}\right] \cdot \left[\begin{array}{c} a \\ \hline b \\ \hline c \end{array}\right] = \left[\begin{array}{c|c|c} 0 & 0 & 0 \\ \hline 0 & 0 & 0 \\ \hline 0 & 0 & P \end{array}\right] \cdot \left[\begin{array}{c} a \\ \hline b \\ \hline c \end{array}\right] \tag{A13}$$

where the superscript T indicates the matrix transpose. Because of the zeros in the right-hand side of equation (A13), the following stability equation can be obtained by matrix operations:

$$\left[[F] - \left[C^T \mid E^T\right] \cdot \left[\begin{array}{c|c} A & B \\ \hline B^T & D \end{array}\right]^{-1} \cdot \left[\begin{array}{c} C \\ \hline E \end{array}\right]\right] \cdot [c] = [P] \cdot [c] \tag{A14}$$

where the superscript -1 indicates the matrix inverse. The left-hand side of equation (A14) can be shown to be symmetric upon consideration of the symmetry properties of the coefficients A, B, C, etc. For specified combinations of the force resultants $\overline{N}_x$ and $\overline{N}_y$, $[P] = \lambda[\overline{P}]$ where λ is a scalar. For example, if the loading is axial compression, $\overline{N}_y = 0$ and $\lambda = \overline{N}_x$; for lateral pressure, $\overline{N}_x = 0$ and $\lambda = p$; and for hydrostatic pressure, $\overline{N}_x = \frac{1}{2}\overline{N}_y$ and $\lambda = p$. In addition, if $\overline{N}_x$ is fixed, the critical value of $\overline{N}_y$ can be found and conversely. In this manner, an interaction curve can be obtained if desired.

The buckling load can be obtained from the stability equation (A14) by the following procedure. When the number of terms in the series expansions of the displacements as well as the number of buckle waves n in the circumferential direction is specified, the lowest eigenvalue can be extracted from equation (A14). The number n is varied over some range until an absolute minimum eigenvalue is found. In the preceding step, it is possible to obtain several relative minimums for the lowest eigenvalue; thus, solutions for a wide range of n values must be investigated before it can be assumed that the absolute minimum has been found. For a given problem, the buckling load is the lowest eigenvalue of the two absolute minimums obtained for the symmetric and antisymmetric modes.

Numerical values were obtained by use of a computer program. Convergence of the solutions was assured to an arbitrary accuracy by comparison of solutions with different numbers of terms in the series expansions of the displacements. The number of terms necessary for convergence to an accuracy of three significant figures varied from three to eight as the shell length was increased.

APPENDIX B

INFLUENCE OF BOUNDARY CONDITIONS

Buckling of Isotropic Cylinders

The significance of the clamped-edge boundary conditions employed herein as applied to the buckling load (eq. (A4)) can be observed by comparing the present solution with existing solutions for axially loaded clamped cylinders and simply supported cylinders. The present solution can be specialized for unstiffened isotropic cylinders by taking the stiffener properties to be zero and making the following substitutions for the orthotropic material constants:

$$\left.\begin{aligned} \mu_x' = \mu_y' = \mu_x = \mu_y = \mu \\ D_x = D_y = Et^3/12 \\ D_{xy} = Gt^3/6 \\ E_x = E_y = Et \\ G_{xy} = Gt \end{aligned}\right\} \tag{B1}$$

The buckling solution thereby obtained is shown in figure 7 along with existing buckling solutions for a membrane prebuckled shape under various boundary conditions. Note that the solutions obtained in reference 12 for clamped and simply supported edges converge when Z is about 10. In contrast, the present results for clamped edges do not converge to the solution for simply supported edges until Z is about 100 because of the additional axial constraint implied by the present boundary conditions. The solution of reference 12 for simply supported cylinders can be shown to have the same boundary conditions as are used in the solution employed herein for simply supported stiffened cylinders (ref. 6). Thus, by analogy, it can be inferred that the substantial effect of clamped edge conditions on the buckling load of even relatively long stiffened cylinders shown in the present results is due in part to axial constraint.

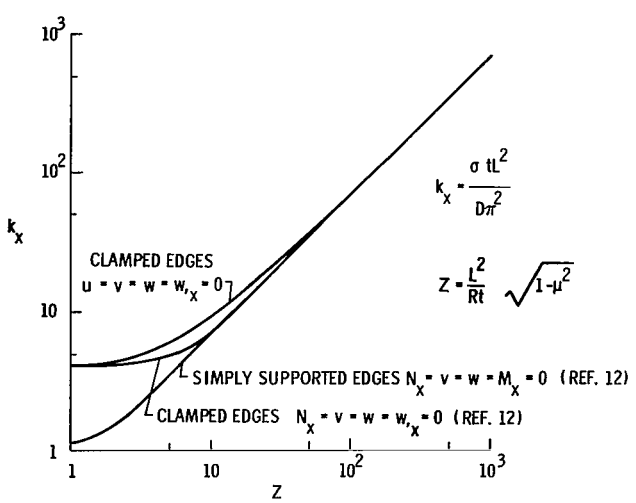

Figure 7.- Buckling of axially compressed isotropic cylinders.

APPENDIX B

Buckling of Axially Compressed Ring-Stiffened Corrugated Cylinders

The present buckling equations can be specialized for ring-stiffened corrugated cylinders by substitution of the following stiffnesses in equations (A1) to (A3):

$$\left.\begin{aligned} E_x &= 2E\left[t_c/(1+\cos\theta_c)\right] \\ G_{xy} &= Gt_c\left(Et_c/E_x\right) \\ D_x &= Et_c p_c^2\left[\sin^2\theta_c/3(1+\cos\theta_c)\right] \\ E_y &= D_y = D_{xy} = \mu'_x = \mu'_y = \mu_x = \mu_y = 0 \end{aligned}\right\} \tag{B2}$$

where t_c is the corrugation thickness, p_c is the corrugation width, and θ_c is the corrugation angle (t_c, p_c, and θ_c shown in fig. 2(c)).

The effect on the buckling load of increasing cylinder length can be studied by obtaining the buckling load of cylinders the length of which is some multiple of the ring spacing. The results of such a procedure are shown in figure 8. In this case, the present clamped-edge solution converges to the simply supported-edge solution of reference 6 much more rapidly (on a percentage basis) for external than for internal rings. At a length-radius ratio L/R of 2, the clamped-edge solution is only 13 percent higher than the simply supported-edge solution for external rings; however, for internal rings, the corresponding value is 45 percent. Thus, boundary conditions are more significant for internal rings than external rings for corrugated cylinders of the configuration considered. This conclusion is interesting because, in contrast, the longitudinally stiffened cylinders considered were found to have substantially greater boundary effects for external stiffeners than for internal stiffeners.

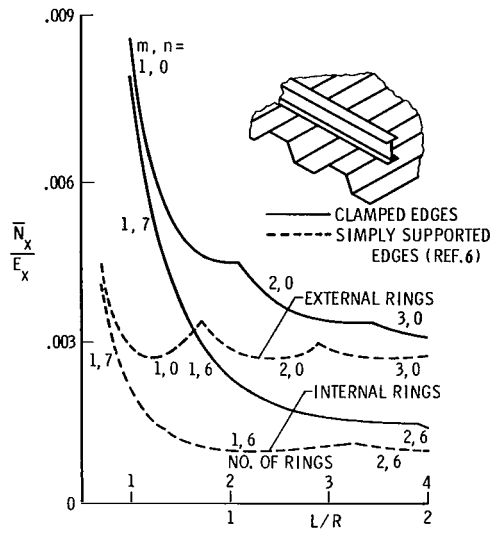

Figure 8.- Buckling of axially compressed, ring-stiffened, corrugated cylinders (as described in fig. 2).

APPENDIX C

CONVERSION OF U.S. CUSTOMARY UNITS TO SI UNITS

The International System of Units (SI) was adopted by the Eleventh General Conference on Weights and Measures, Paris, October 1960, in Resolution No. 12 (ref. 8). Conversion factors for the units used herein are given in the following table:

Physical quantity	U.S. Customary Unit	Conversion factor (*)	SI Unit
Length	in.	0.0254	meters (m)
Force	kips	4.448×10^3	newtons (N)
Stress	ksi = kips/in^2	6.895×10^6	newtons per square meter (N/m^2)

*Multiply value given in U.S. Customary Unit by conversion factor to obtain equivalent value in SI Unit.

Prefixes to indicate multiple of units are as follows:

Prefix	Multiple
centi (c)	10^{-2}
kilo (k)	10^3
mega (M)	10^6

REFERENCES

1. Van der Neut, A.: The General Instability of Stiffened Cylindrical Shells Under Axial Compression. Rept. S. 314, Nat. Aeron. Res. Inst. (Amsterdam), 1947.

2. Baruch, M.; and Singer, J.: Effect of Eccentricity of Stiffeners on the General Instability of Stiffened Cylindrical Shells Under Hydrostatic Pressure. J. Mech. Eng. Sci., vol. 5, no. 1, 1963, pp. 23-27.

3. Hedgepeth, John M.; and Hall, David B.: Stability of Stiffened Cylinders. AIAA J., vol. 3, no. 12, Dec. 1965, pp. 2275-2286.

4. Crawford, R. F.: Effects of Asymmetric Stiffening on Buckling of Shells. AIAA Paper No. 65-371, Am. Inst. Aeron. Astronaut., July 1965.

5. Stuhlman, C.; DeLuzio, A.; and Almroth, B.: Influence of Stiffener Eccentricity and End Moment on Stability of Cylinders in Compression. AIAA J., vol. 4, no. 5, May 1966, pp. 872-877. (Also presented in proceedings of the AIAA 6th Structures and Materials Conference (Palm Springs, California), Apr. 1965, pp. 117-125.)

6. Block, David L.; Card, Michael F.; and Mikulas, Martin M., Jr.: Buckling of Eccentrically Stiffened Orthotropic Cylinders. NASA TN D-2960, 1965.

7. Card, Michael F.: Preliminary Results of Compression Tests on Cylinders With Eccentric Longitudinal Stiffeners. NASA TM X-1004, 1964.

8. Mechtly, E. A.: The International System of Units – Physical Constants and Conversion Factors. NASA SP-7012, 1964.

9. Wang, Chi-Teh: Applied Elasticity. McGraw-Hill Book Co., Inc., New York, 1953, p. 89.

10. Peterson, James P.; and Dow, Marvin B.: Compression Tests on Circular Cylinders Stiffened Longitudinally by Closely Spaced Z-Section Stringers. NASA MEMO 2-12-59L, 1959.

11. Frazer, R. A.; Duncan, W. J.; and Collar, A. R.: Elementary Matrices. Cambridge Univ. Press, 1950, pp. 224-228.

12. Batdorf, S. B.; Schildcrout, Murry; and Stein, Manuel: Critical Stress of Thin-Walled Cylinders in Axial Compression. NACA Rept. 887, 1947. (Formerly NACA TN 1343.)

"The aeronautical and space activities of the United States shall be conducted so as to contribute ". . . to the expansion of human knowledge of phenomena in the atmosphere and space. The Administration shall provide for the widest practicable and appropriate dissemination of information concerning its activities and the results thereof."

—NATIONAL AERONAUTICS AND SPACE ACT OF 1958

NASA SCIENTIFIC AND TECHNICAL PUBLICATIONS

TECHNICAL REPORTS: Scientific and technical information considered important, complete, and a lasting contribution to existing knowledge.

TECHNICAL NOTES: Information less broad in scope but nevertheless of importance as a contribution to existing knowledge.

TECHNICAL MEMORANDUMS: Information receiving limited distribution because of preliminary data, security classification, or other reasons.

CONTRACTOR REPORTS: Technical information generated in connection with a NASA contract or grant and released under NASA auspices.

TECHNICAL TRANSLATIONS: Information published in a foreign language considered to merit NASA distribution in English.

TECHNICAL REPRINTS: Information derived from NASA activities and initially published in the form of journal articles.

SPECIAL PUBLICATIONS: Information derived from or of value to NASA activities but not necessarily reporting the results of individual NASA-programmed scientific efforts. Publications include conference proceedings, monographs, data compilations, handbooks, sourcebooks, and special bibliographies.

Details on the availability of these publications may be obtained from:

SCIENTIFIC AND TECHNICAL INFORMATION DIVISION

NATIONAL AERONAUTICS AND SPACE ADMINISTRATION

Washington, D.C. 20546